Direct Observation of Resonant Scattering Phase Shifts and Their Energy Dependence

Stephen D. Gensemer,* Ross B. Martin-Wells, Aaron W. Bennett, and Kurt Gibble
Department of Physics, The Pennsylvania State University, University Park, Pennsylvania 16802, USA
(Received 24 September 2012; published 26 December 2012)

We scan the collision energy of two clouds of cesium atoms between 12 and 50 μK in an atomic fountain clock. By directly detecting the difference of s-wave scattering phase shifts, we observe a rapid variation of a scattering phase shift through a series of Feshbach resonances. At the energies we use, resonances that overlap at threshold become resolved. Our statistical phase uncertainty of 8 mrad can be improved in future precision measurements of Feshbach resonances to accurately determine the Cs-Cs interactions, which may provide stringent limits on the time variation of fundamental constants.

DOI: 10.1103/PhysRevLett.109.263201 PACS numbers: 34.50.Cx, 06.30.Ft

Feshbach scattering resonances occur when the continuum state of two colliding particles couples to a bound state (Fig. 1) [1]. Feshbach resonances have found wide applicability in dilute, ultracold, atomic, and molecular gases because they provide an accessible control of the interparticle interactions [2–6]. Feshbach's elegant treatment of scattering resonances showed that scattering phase shifts, and hence cross sections, change rapidly as the collision energy tunes through resonance. The rapid phase change is a general feature of resonance phenomena and the resonant energy dependence of cross sections has been observed in a variety of experiments, including neutron and electron scattering and photodetachment [7–9]. In ultracold gases, so far magnetic fields have been used to tune resonances to threshold, changing the energy of the bound state by vertically translating the grey potential in Fig. 1, instead of tuning the collision energy [3–11]. Here, we scan the collision energy between two ultracold clouds of cesium atoms in an atomic clock and directly observe the scattering phase shift [12] through a series of scattering resonances. Increasing the collision energy allows us to resolve resonances that overlap at threshold. Precise measurements of scattering phase shifts through a resonance will very accurately determine the resonance position, giving a highly precise determination of the atomic interactions [5] and a potential route to stringent limits on the time variation of fundamental constants [13,14].

We directly measure scattering phase shifts by preparing cesium atoms in coherent superpositions of the two clock states and detecting the phase shift of these coherences after the clock atoms scatter off atoms prepared in a pure 'target' state (Fig. 2 inset) [12]. When the $|F = 3, m_F = 0\rangle$ ($|40\rangle$) clock state scatters off the target atoms, it acquires a scattering phase shift $\delta_3(\delta_4)$. The phase of the clock coherence, the superposition of $|30\rangle$ and $|40\rangle$, precesses as hands on a clock. The scattering causes the phase of the coherence to jump by the difference of the scattering phase shifts, $\Phi = \delta_4 - \delta_3$ [12], represented by the time difference between the ring of scattered clocks and the unscattered clock in the Fig. 2 inset. We directly detect Φ as a phase shift of the clock's Ramsey fringes as in Fig. 2(b). To be sensitive to the s-wave phase shifts, we detect atoms that scatter near 90°, using the Doppler shift of a stimulated-Raman transition [12,15]. By also measuring the cross sections for each clock state on $|32\rangle$, we isolate the scattering resonances to only the $|32\rangle \otimes |40\rangle$ channel, and exclude the $|32\rangle \otimes |30\rangle$ channel.

In our fountain clock, we launch two clouds of cesium atoms with short time delays, 6.5–11 ms, to give collision energies between 12 and 50 μK [12,16]. A series of microwave pulses in three microwave cavities state prepares the atoms in the first cloud (C1) in a desired $|3, m_F = 1, 2, 3\rangle$ target state and the second cloud (C2) in $|41\rangle$. A two-photon stimulated Raman transition transfers a 270 nK wide slice of the C2 vertical velocity distribution from $|41\rangle$ to $|30\rangle$.

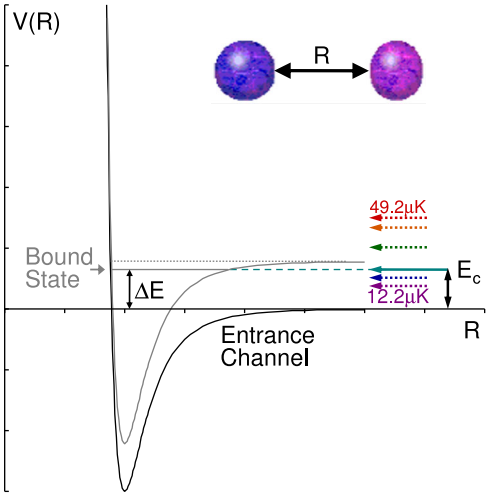

FIG. 1 (color online). A Feshbach scattering resonance occurs when the collision energy E_c (aqua solid arrow) has the same energy as a bound state of the two particles. We scan the collision energy from 12 to 49 μK (dashed arrows) and observe a series of Cs-Cs scattering resonances. The schematic grey potential energy surface, as a function of internuclear distance R, can also be shifted vertically by changing the magnetic field B, which instead shifts the energy of the bound state ΔE. Throughout the Letter we use energy units of E_c/k_B.

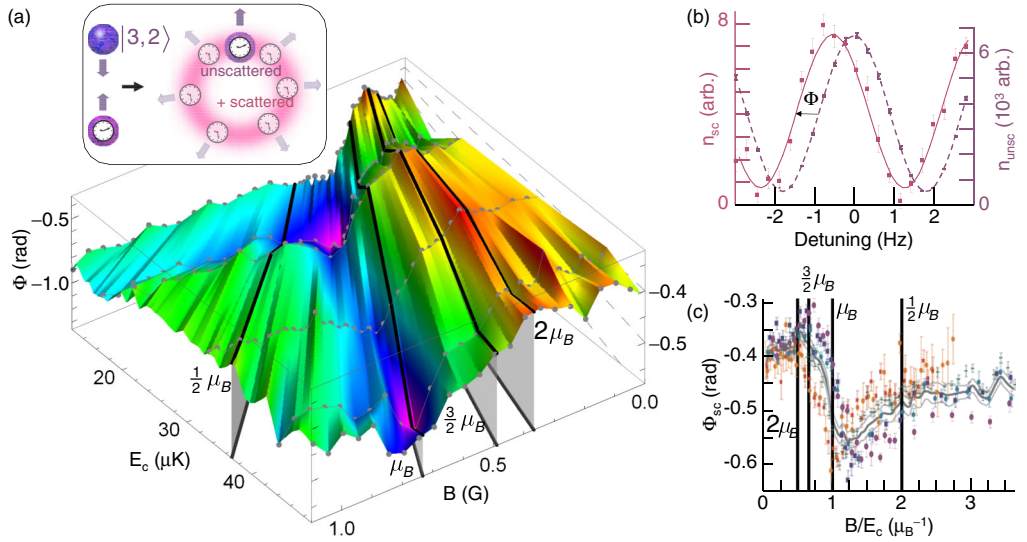

FIG. 2 (color online). (Inset) Clock atoms in a coherent superposition of two internal clock states scatter off of target atoms (in $|32\rangle$), giving each clock state a quantum scattering phase shift. The phase of the clock coherence is represented by the time of the scattered and unscattered clocks. For scattered atoms, the clock phase is shifted by the difference of the quantum scattering phase shifts Φ of the two clock states. (a) Resonances of quantum scattering phase shifts versus collision energy E_c and magnetic field B. The measured phase differences Φ (grey dots) are the difference of s-wave phase shifts for the cesium clock states scattering off cesium atoms prepared in $|32\rangle$. The black lines illustrate the allowed differences of magnetic moments for an $l = 0$ halo molecular state. Features at μ_B and $3/2\mu_B$ suggest the bound states are resonant near $E_c = 0$. For clarity, the vertical scale varies linearly with E_c. (b) Atomic clock transition probability with two $\pi/2$ pulses for scattered (solid) and unscattered (dashed) atoms at $E_c = 12.2$ μK and $B = 0.3$ G. The phase shift Φ is plotted in (a). Each point represents the average of 18 fountain launch measurements, plus background measurements [16]. (c) Φ from (a) versus B, scaled by E_c, yields essentially the same shape for all E_c, as expected for the peculiar case of bound states near threshold. Here the amplitude of Φ is scaled by the spread of collision energies δE as discussed in the text. The black vertical lines represent the same magnetic moments in (a) and the data point colors are from Fig. 1. The weighted average of Φ_{sc} versus B gives an approximate reference shape for all energies (grey curves).

Interleaved with these transitions are clearing laser pulses tuned to the $6s_{1/2}, F = 4 \rightarrow 6p_{3/2}, F' = 5'$ and $3 \rightarrow 2'$ transitions that remove unselected atoms. The microwave clock cavity then prepares C2 atoms in a coherent superposition of $|30\rangle$ and $|40\rangle$ and the clouds collide near the apogee. A small fraction of the atoms in the clouds scatter, forming an expanding spherical shell of atoms, whose coherence is shifted by the difference of their s-wave scattering phase shifts. When the scattered shell is centered in the clock cavity, a second $\pi/2$ clock pulse converts the phase of the scattered atoms' coherence into a population difference between $|30\rangle$ and $|40\rangle$. A clearing pulse then removes the C1 target atoms and the atoms in $|30\rangle$. To detect the scattered atom's Ramsey fringe, we velocity-selectively transfer atoms that scatter near 90° from $|40\rangle$ to $|30\rangle$. After clearing and optical pumping pulses remove $F = 4$ atoms, a laser beam tuned to $F = 4 \rightarrow F' = 5$ excites the atoms and we collect the fluorescence with a lens and photodiode. To detect the phase shift of the scattered atoms, we use the phase of the unscattered atoms as a reference [Fig. 2(b)] and, to measure and remove backgrounds, we use a pump-probe technique where we inhibit the selection of C1, C2, or both clouds [12].

Figure 2 shows a large and rapid variation of the scattering phase shifts Φ as a function of collision energy E_c and magnetic field B for target atoms prepared in $|32\rangle$. Feshbach resonances generally tune with both the collision energy E_c and magnetic field B, with a slope in the $E_c - B$ plane that is given by the difference of the magnetic moments of the coupled bound state and the incident channel. The black lines in Fig. 2 show the slopes for magnetic moments of $1/2$, 1, $3/2$, and 2 Bohr magnetons, μ_B. Strikingly, all of the features we observe for $|32\rangle$ target atoms, as well as $|33\rangle$ and $|31\rangle$ targets below, follow one of these slopes with intercepts that are near the origin of the $E_c - B$ plane. For a single narrow Feshbach resonance, the observed width would be proportional to the spread of collision energies, roughly proportional to $E_c^{1/2}$. Instead, the features in Fig. 2 follow the black lines, scaling linearly with energy, as expected if there were two (or more) Feshbach resonances, with different magnetic moments. The small intercepts of the features suggest that the bound states have small binding energies (at $B = 0$), lying very close to threshold, $E_c = 0$. Further, if the slopes are multiples of $\mu_B/2$, it is likely that the bound states are halo molecular states, which have magnetic moments that are essentially the same as those for free atoms. For s-wave Feshbach resonances, the halo states asymptotically correspond to $|31\rangle \otimes |41\rangle$, $|30\rangle \otimes |42\rangle$, $|3,-1\rangle \otimes |43\rangle$, and $|3,-2\rangle \otimes |44\rangle$ at large internuclear separations. The magnetic

moments for these halo states near threshold give resonance positions near the black lines in Fig. 2. We note that coupling to these states conserves the total z angular momentum, the total molecular M_F, as required for an s-wave resonance. If the Feshbach resonances had an angular momentum higher than s-wave, other total M_F's would be allowed, with corresponding differences of magnetic moments. We have not observed these for target atoms in $|32\rangle$, or $|31\rangle$ or $|33\rangle$.

The shape of the resonant phase shifts in Fig. 2(a) versus magnetic field is remarkably similar for all of our collision energies E_c. If the corresponding bound states for all the Feshbach resonances have the same binding energy $\Delta E \approx 0$, scaling the magnetic field B as $B/(E_c + \Delta E)$ should align all of the resonances, as in Fig. 2(c). As for any general resonance, the scattering phase shift goes through π as we sweep across a resonance. However, if each resonance is narrower than our rms spread of collision energies δE, the peak-to-peak phase excursions will be smaller, with an amplitude proportional to δE^{-1}. We prepare the atoms in each cloud with a mean temperature of 590 nK, which gives $\delta E = 3.2\ \mu$K at $E_c = 12.2\ \mu$K and a larger $\delta E = 8.9\ \mu$K at 49.2 μK, proportional to $E_c^{1/2}$ [16]. Thus, the observed peak-to-peak phase excursions are smaller for large E_c. With this phase and B/E_c scaling, the magnetic field dependence through the series of the Feshbach resonances in Fig. 2(c) has nearly the same form over our range of energies. Averaging this scaled data gives a function (gray curve) to compare to the measured phase versus E_c and B. Interestingly, the gray curve and the data for each E_c show the statistical significance of a nearly flat region between $3/2$ and $1\mu_B$; the phase steeply decreases, flattens, and then continues steeply down again for all of the collision energies, which can occur if there are resonances near $3/2$ and $1\mu_B$. We speculate that a Feshbach resonance should also exist near $1/2\mu_B$. If it does, it is apparently sufficiently narrow that we do not resolve it for $|32\rangle$ targets, but the bound state coupling is evidently larger for $|33\rangle$ target atoms as we observe this resonance below.

Figure 3(a) depicts the bound state energies versus magnetic field (black lines), for multiples of $\mu_B/2$ with $\Delta E = 0$. The intersections of these bound state energies with our six chosen collision energies (horizontal lines) represent the positions of potential Feshbach resonances. In Fig. 3(c) the scattering phase shift difference for the $|32\rangle$ target atoms is shown for each E_c versus B, along with the grey curve, the average of the scaled data in Fig. 2(c). While this curve describes the data quite well, there are deviations that vary systematically with energy. These deviations could be due to the multiple bound states having significantly different binding energies ΔE. In addition, biases in the effective collision energy can occur since the $|32\rangle \otimes |40\rangle$ and $|32\rangle \otimes |30\rangle$ scattering cross sections are energy dependent. Both contribute to an energy bias of the scattered atoms that we detect. Full coupled-channels calculations yield both the phase and cross-section variations and a comparison of these

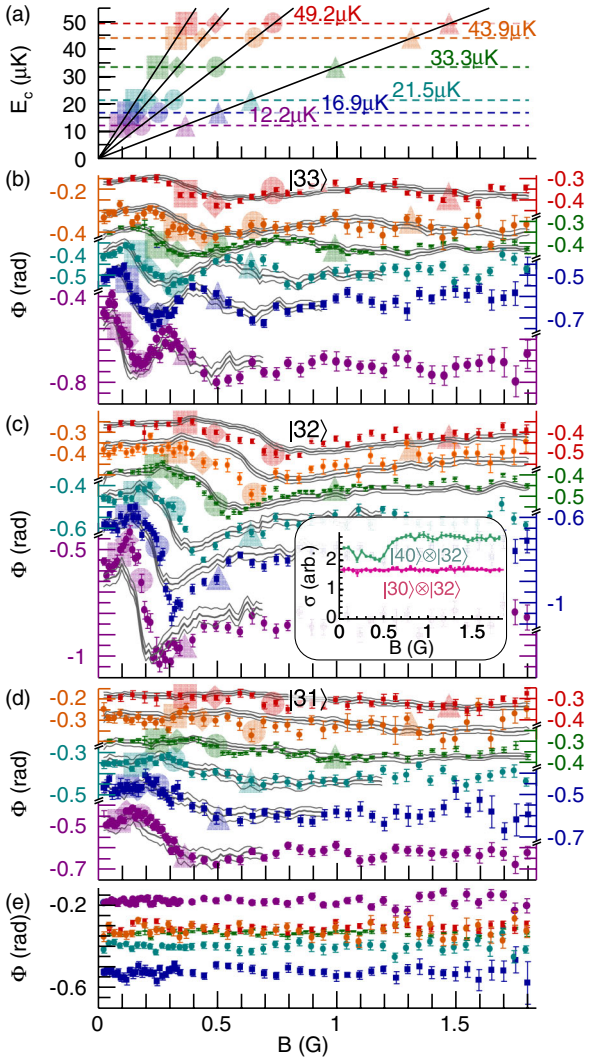

FIG. 3 (color online). (a) Positions of Feshbach scattering resonances versus E_c and B, denoted by the large symbols (squares, diamonds, circles, triangles), for molecular bound states that are resonant at threshold, with magnetic moments that are different from those for bare atoms by (1/2, 1, 3/2, 2) μ_B. The experimental E_c's are depicted by the dashed horizontal lines. (b–e) Measured difference of s-wave scattering phase shifts for six collision energies E_c versus magnetic field B, for target atoms in $|33\rangle$, $|32\rangle$, $|31\rangle$, and $|3, -3\rangle$. As in Fig. 2(a), the scattering resonances shift with E_c and B. In (b–d) at all energies, scattering resonances occur near the symbols from (a) (see text). (c) Inset: The scattering cross section of $|32\rangle$ on $|40\rangle$ (magenta) shows scattering resonances, whereas $|32\rangle$ on $|30\rangle$ does not. In (e), note that the target for 12.2 μK is $|44\rangle$.

with such measurements can precisely test and improve our knowledge of the Cs-Cs molecular interactions. We find that all the resonances, when extrapolated to $B = 0$, are consistent with binding energies between 0 and 10 μK. This is consistent with a previous observation of frequency shift cross sections at threshold, which appeared to indicate the existence of one or two overlapping Feshbach resonances of states with binding energies of $\Delta E = 0 < 0.5\ \mu$K at $B = 0$ [17,18].

Figures 3(b) and 3(d) show the measured phase shift differences for target atoms in $|33\rangle$ and $|31\rangle$. The $|33\rangle$ and $|31\rangle$ scattering shows features near the magnetic moments of the same halo molecular states as $|32\rangle$. Here, $|33\rangle$ scattering has a clear resonance that asymptotically corresponds to $\approx \mu_B/2$ for the $|32\rangle \otimes |41\rangle$ exit channel.

Figure 3(e) shows the phase difference for a $|3,-3\rangle$ target, which has no obvious resonances. We use this channel to measure small magnetic field gradients throughout the atomic trajectories in our fountain clock [16], which make a clock precision of 8 mrad challenging at high magnetic fields. While the clock transition, $|30\rangle \rightarrow |40\rangle$, has no linear Zeeman shift, it has a quadratic Zeeman shift of 427 Hz/G^2. At $B = 1.8$ G, the quadratic Zeeman shift is 1.4 kHz. With a typical Ramsey fringe linewidth of 4.4 Hz for 33.3 μK, an 8 mrad phase uncertainty corresponds to a frequency uncertainty of 11 mHz, and a magnetic field uncertainty of 7 μG. Since we sweep over a wide range of magnetic fields, our clock has no magnetic shielding. To achieve this precision, a flux-gate magnetometer and control system actively stabilizes the vertical field, reducing the background fluctuations of approximately 3 mG. We use the unscattered clock atoms [Fig. 2 inset and Fig. 2(b)] to measure the quadratic Zeeman shift along the fountain trajectory. Because the s-wave halo of scattered atoms follows a different trajectory than the unscattered atoms, magnetic field variations in our clock produce a phase shift of order 100 mrad for $B > 1$ G. We therefore interleave measurements of $|44\rangle$ or $|3,-3\rangle$ target atoms, prepared with a nonadiabatic magnetic field reversal [Fig. 3(e)]. Since the phase shifts for these states show no scattering resonances, we use $|3,-3\rangle$ and $|44\rangle$ targets to measure and correct the magnetic field variations for the scattered halo for other target states [16].

We note that scattering phase shifts have sharp steps as inelastic scattering channels close. While scattering phase shifts wrap through π at Feshbach resonances, phase steps at inelastic thresholds do not, and are often small [19,20]. The phase excursions we observe are large, even after thermally averaging. Therefore, these are almost certainly Feshbach resonances, along with smaller contributions from inelastic thresholds. The peak-to-peak phase excursions we see are consistent with Feshbach widths of order of several mG. If the widths were significantly wider (narrower), our spread of collision energies would yield larger (smaller) peak-to-peak phase excursions.

The spread of collision energies for two colliding clouds is significantly larger than the temperatures of each cloud for high collision energies. The spread is $\delta E = [E_0(T_1 + T_2) + 3/8(T_1 + T_2)^2]^{1/2}$, where E_0 is the collision energy due to the relative velocities of the two clouds ($T = 0$ limit), and T_1 and T_2 are the temperatures of each cloud [16]. In our fountain clock, the atoms are cooled using degenerate sideband cooling in a moving-frame optical lattice [21]. The first cloud's temperature (≈ 790 nK) is higher than the second cloud's (≈ 390 nK) since the first cloud, multiply loaded in a double magneto-optical trap (MOT) [12], has more atoms than the second, which is launched directly from a vapor-cell MOT.

In conclusion, we directly observe a rapid variation of s-wave scattering phase shifts as we scan the collision energy through a series of Feshbach resonances. Reducing the spread of collision energies could yield even more precise measurements of the phase shifts and the positions of the Feshbach resonances. To resolve these overlapping resonances, the collision energy has to be of order 10 μK. Currently, our state-preparation velocity selects the second cloud to 270 nK and this velocity selection can be narrower. Adding a narrow velocity selection of the first cloud will help even more. Since only the velocity spread along the collision axis contributes significantly to the spread of collision energies, cooling in one dimension is sufficient [22]. Alternatively, a sample can be evaporatively cooled, split, and then accelerated to collide [23,24]. Higher energy resolution and a thorough evaluation of systematic errors will lead to a highly precise determination of the cesium interactions [5,25,26]. In turn, these can place stringent limits on the time variations of underlying fundamental forces [13,14].

We acknowledge discussions with S. Kokkelmans and E. Tiesinga and financial support from the NSF and Penn State.

*Present address: Centre for Engineered Quantum Systems, School of Physics, The University of Sydney, NSW 2006, Australia.

[1] H. Feshbach, Ann. Phys. (N.Y.) **19**, 287 (1962).
[2] E. Tiesinga, A. J. Moerdijk, B. J. Verhaar, and H. T. C. Stoof, Phys. Rev. A **46**, R1167 (1992).
[3] S. Inouye, M. R. Andrews, J. Stenger, H.-J. Miesner, D. M. Stamper-Kurn, and W. Ketterle, Nature (London) **392**, 151 (1998).
[4] J. L. Roberts, N. R. Claussen, S. L. Cornish, E. A. Donley, E. A. Cornell, and C. E. Wieman, Phys. Rev. Lett. **86**, 4211 (2001).
[5] C. Chin, V. Vuletić, A. J. Kerman, S. Chu, E. Tiesinga, P. J. Leo, and C. J. Williams, Phys. Rev. A **70**, 032701 (2004).
[6] C. Chin, R. Grimm, P. Julienne, and E. Tiesinga, Rev. Mod. Phys. **82**, 1225 (2010).
[7] R. E. Peterson, H. H. Barschall, and C. K. Bockelman, Phys. Rev. **79**, 593 (1950).
[8] D. Spence and T. Noguchi, J. Chem. Phys. **63**, 505 (1975).
[9] H. C. Bryant, B. D. Dieterle, J. Donahue, H. Sharifian, H. Tootoonchi, D. M. Wolfe, P. A. M. Gram, and M. A. Yates-Williams, Phys. Rev. Lett. **38**, 228 (1977).
[10] E. L. Hazlett, Y. Zhang, R. W. Stites, and K. M. O'Hara, Phys. Rev. Lett. **108**, 045304 (2012).
[11] C. Kohstall, M. Zaccanti, M. Jag, A. Trenkwalder, P. Massignan, G. M. Bruun, F. Schreck, and R. Grimm, Nature (London) **485**, 615 (2012).
[12] R. A. Hart, X. Xu, R. Legere, and K. Gibble, Nature (London) **446**, 892 (2007).

[13] C. Chin and V. V. Flambaum, Phys. Rev. Lett. **96**, 230801 (2006).
[14] A. Borschevsky, K. Beloy, V. V. Flambaum, and P. Schwerdtfeger, Phys. Rev. A **83**, 052706 (2011).
[15] M. Kasevich, D. S. Weiss, E. Riis, K. Moler, S. Kasapi, and S. Chu, Phys. Rev. Lett. **66**, 2297 (1991).
[16] See Supplemental Material at http://link.aps.org/supplemental/10.1103/PhysRevLett.109.263201 for more details about the experimental sequence, a discussion of the data analysis and systematic errors, and scaled plots [Fig. 2(c)] for $|33\rangle$ and $|31\rangle$ target atoms.
[17] H. Marion, S. Bize, L. Cacciapuoti, D. Chambon, F. Pereira dos Santos, G. Santarelli, P. Wolf, A. Clairon, A. Luiten, M. Tobar, S. Kokkelmans, and C. Salomon, arXiv:physics/0407064.
[18] D. J. Papoular, S. Bize, A. Clairon, H. Marion, S. J. J. M. F. Kokkelmans, and G. V. Shlyapnikov, Phys. Rev. A **86**, 040701(R) (2012).
[19] S. J. J. M. F. Kokkelmans (private communication).
[20] E. Tiesinga (private communication).
[21] P. Treutlein, K. Y. Chung, and S. Chu, Phys. Rev. A **63**, 051401 (2001).
[22] H. J. Lee, C. S. Adams, M. Kasevich, and S. Chu, Phys. Rev. Lett. **76**, 2658 (1996).
[23] N. R. Thomas, Niels Kjærgaard, P. S. Julienne, and A. C. Wilson, Phys. Rev. Lett. **93**, 173201 (2004).
[24] C. Buggle, J. Léonard, W. von Klitzing, and J. T. M. Walraven, Phys. Rev. Lett. **93**, 173202 (2004).
[25] K. Szymaniec, W. Chałupczak, E. Tiesinga, C. J. Williams, S. Weyers, and R. Wynands, Phys. Rev. Lett. **98**, 153002 (2007).
[26] Ph. Laurent, M. Abgrall, Ch. Jentsch, P. Lemonde, G. Santarelli, A. Clairon, I. Maksimovic, S. Bize, Ch. Salomon, D. Blonde, J. F. Vega, O. Grosjean, F. Picard, M. Saccoccio, M. Chaubet, N. Ladiette, L. Guillet, I. Zenone, Ch. Delaroche, and Ch. Sirmain, Appl. Phys. B **84**, 683 (2006).